Buckling Analysis of S, P and E Functionally Graded Plate Using New Hyperbolic Shear Deformation Theory

Ambili R G, Parvathy U
Civil Engineering Department
Mar Baselios College of Engineering and Technology
Thiruvananthapuram, India
ambilishivin@gmail.com, parvathyu89@gmail.com

Abstract—**Functionally Graded (FGM) plate is a two or more component composite plate having a compositional gradient which varies continuously from one component to the other throughout the thickness direction. Due to the continuous change in material properties of an FGM, the interface between the two materials disappear but the characteristics of the two or more materials are preserved. Subsequently the stress singularity at the interface is eliminated and thus the bonding strength is enhanced. This new concept of engineering the materials microstructure marks the beginning of a revolution both in the material science and in the area of mechanics of material. Various theories can be used for the analysis of isotropic and composite plates. The present study explores the feasibility of a New Hyperbolic Shear Deformation Theory (NHPSDT) for the buckling analysis of simply supported functionally graded plate subjected to uniaxial inplane compressive forces. The theory accounts for a hyperbolic distribution of the transverse shear strains across the thickness without using any shear correction factors. Buckling analysis of FGM plate is done using the three idealization techniques namely Power law (PFGM), Sigmoid (SFGM) and Exponential (EFGM) function. A closed form solution is proposed for the buckling analysis of simply supported FG plates using the NHPSDT. The effects of aspect ratio, E1/E2 ratio, b/h ratio and material parameter on the buckling behaviour of FGM plate is investigated. Finally the critical buckling load obtained for the SFGM plate is also compared with that obtained for an isotropic plate.**

Keywords-Functionally graded material; New hyperbolic shear deformation theory; Power law; Sigmoid and Exponential law function

I. INTRODUCTION

Functionally Graded Material (FGM) was first introduced in 1984 by a group of material scientists in Japan as ultrahigh temperature resistant materials for aircraft, space vehicles and other engineering applications. FGM is a new composite material in which there are two or more constituent phases with smooth and continuously varying composition. In tradi-tional layered composites stress singularities may occur at the interface between two different materials due to the mismatch of materials especially in a high temperature environment. Therefore the concept of FGM was introduced to satisfy the demand of ultra high temperature environment and to eliminate the stress singularities.

The computational models developed for predicting the response of functionally graded (FG) plates can be developed using theories classified under three main categories: Classical plate theory (CPT), first order shear deformation theory (FSDT) and higher order shear deformation theories (HSDT) which include third order shear deformation theory (TSDT). CPT neglects the shear deformation and provides accurate results for thin plates. It overestimate the buckling loads for thick plates. FSDT accounts for the shear deformations by use of shear correction factor and provides satisfactory results for moderately thick plates. But it is difficult to get the correct value for the shear correction factor. To overcome this difficulty HSDT developed with five unknowns to predict the response of FG plates.

This paper uses a New Hyperbolic Shear Deformation Theory (NHPSDT) for the buckling analyses of FG plates. This theory is based on the assumption that the in-plane and transverse displacements consists of bending and shear parts. Unlike the other shear deformation theories this theory has only four unknowns. Material property of the FG plates is assumed to vary according to the Power law, Sigmoid and Exponential law distribution of the volume fraction of the constituents. Equation of the equilibrium is derived using the principle of virtual displacement. The closed form solution is obtained for the simply supported plates. Numerical examples are presented to verify the accuracy of the proposed theory in predicting the buckling responses of FG plates.

II. THEORETICAL FORMULATION

Consider an FG plate of thickness **h**. The xy plane is taken to be the undeformed mid plane of the plate with z axis positive upward from the mid plane.

A. Displacement fields and Strains

The assumed displacement field is as follows,

$$u(x,y,z) = u_0(x,y) - z\frac{\partial w_b}{\partial x} - f(z)\frac{\partial w_s}{\partial x} \qquad (1)$$

$$v(x,y,z) = v_0(x,y) - z\frac{\partial w_b}{\partial y} - f(z)\frac{\partial w_s}{\partial y} \quad (2)$$

$$w(x,y,z) = w_b(x,y) + w_s(x,y) \quad (3)$$

where u_0 and v_0 are the mid-plane displacements of the plate in the x and y direction respectively; w_b and w_s are the bending and shear components of transverse displacement respectively. The hyperbolic function which is used for the representation of the transverse shear deformation is given in (4).

$$f(z) = z[1 + \frac{3\pi}{2}\sec \mathbf{h}^2(\frac{1}{2})] - \frac{3\pi}{2}\mathbf{h}\tanh(\frac{z}{\mathbf{h}}) \quad (4)$$

The kinematic relations can be obtained as follows:

$$\varepsilon_x = \varepsilon_x^0 + zK_x^b + f(z)K_x^s \quad (5)$$

$$\varepsilon_y = \varepsilon_y^0 + zK_y^b + f(z)K_y^s$$

$$\gamma_{xy} = \gamma_y^0 + zK_{xy}^b + f(z)K_{xy}^s$$

$$\gamma_{yz} = g(z)\gamma_{yz}^s \ , \ \gamma_{xz} = g(z)\gamma_{xz}^s \ , \ \varepsilon_z = 0$$

where

$$\varepsilon_x^0 = \frac{\partial u_0}{\partial x}, \varepsilon_y^0 = \frac{\partial v_0}{\partial y} \quad (6)$$

$$K_x^b = -\frac{\partial^2 w_b}{\partial x^2}, \ K_y^b = -\frac{\partial^2 w_b}{\partial y^2}$$

$$K_x^s = -\frac{\partial^2 w_s}{\partial x^2}, \ K_y^s = -\frac{\partial^2 w_s}{\partial y^2}$$

$$\gamma_{xy}^0 = \frac{\partial u_0}{\partial y} + \frac{\partial v_0}{\partial x}$$

$$K_{xy}^b = -2\frac{\partial^2 w_b}{\partial x \partial y}, \ K_{xy}^s = -2\frac{\partial^2 w_s}{\partial x \partial y}$$

$$\gamma_{yz}^s = \frac{\partial w_s}{\partial y}, \gamma_{xz}^s = \frac{\partial w_s}{\partial x}$$

$$g(z) = 1 - f'(z)$$

$$f'(z) = \frac{df(z)}{dz}$$

B. Constitutive relations

In FGM, material property gradation is considered through the thickness using Power law, Sigmoid and Exponential law and the expressions for each is given in (7),(8) and (9) respectively which represents the profile for the volume fraction.

$$E(z) = E_t g(z) + E_b(1 - g(z)) \quad (7)$$

$$g(z) = (\frac{z}{h} + \frac{1}{2})^n$$

$$E(z) = E_t g_1(z) + E_b(1 - g_1(z)), 0 \le z \le h/2 \quad (8)$$

$$E(z) = E_t g_2(z) + E_b(1 - g_2(z)), -h/2 \le z \le 0$$

$$g_1(z) = 1 - \frac{1}{2}(1 - \frac{2z}{h})^n, 0 \le z \le h/2$$

$$g_2(z) = \frac{1}{2}(1 + \frac{2z}{h})^n, -h/2 \le z \le 0$$

$$E(z) = Ae^{B(z+\frac{h}{2})} \quad (9)$$

$$A = E_b$$

$$B = \frac{1}{h} ln \frac{E_b}{E_t}$$

Where E denotes modulus of elasticity. E_t and E_b denote the modulus of elasticity at the top and bottom faces of the plate respectively and 'n' is the material parameter which represent the proportion of different constituents along the thickness direction. It is assumed that Poisson's ratio 'ν' to be a constant. The linear constitutive relations are,

$$\begin{bmatrix} \sigma_x \\ \sigma_y \\ \tau_{yz} \\ \tau_{xz} \\ \tau_{xy} \end{bmatrix} = \begin{bmatrix} Q_{11} & Q_{12} & 0 & 0 & 0 \\ Q_{12} & Q_{11} & 0 & 0 & 0 \\ 0 & 0 & Q_{44} & 0 & 0 \\ 0 & 0 & 0 & Q_{55} & 0 \\ 0 & 0 & 0 & 0 & Q_{66} \end{bmatrix} \begin{bmatrix} \varepsilon_x \\ \varepsilon_y \\ \gamma_{yz} \\ \gamma_{xz} \\ \gamma_{xy} \end{bmatrix} \quad (10)$$

where

$$Q_{11} = \frac{E(z)}{1 - \nu^2} \quad (11)$$

$$Q_{44} = Q_{55} = Q_{66} = \frac{E(z)}{2(1+\nu)}$$

$$Q_{12} = \nu Q_{11}$$

C. Governing equation

The governing equations of equilibrium can be derived by using the principle of virtual displacements. The principle of virtual work in the present case yields.

$$\int_{-\frac{h}{2}}^{\frac{h}{2}} \int_A [\sigma_x \delta\varepsilon_x + \sigma_y \delta\varepsilon_y + \tau_{xy}\delta\gamma_{xy} + \tau_{yz}\delta\gamma_{yz} + \tau_{xz}\delta\gamma_{xz}] dA dz + \int_A [N_x^0 \frac{\partial w}{\partial x}\frac{\partial \delta w}{\partial x} + N_y^0 \frac{\partial w}{\partial y}\frac{\partial \delta w}{\partial y} + 2N_{xy}^0 \frac{\partial w}{\partial x}\frac{\partial \delta w}{\partial y}] dA = 0 \quad (12)$$

Integrating through the thickness of the plate (12) can be rewritten as (13).

$$\int_A [N_x \delta\epsilon_x^0 + N_y \delta\epsilon_y^0 + N_{xy}\delta\epsilon_{xy}^0 + M_x^b \delta K_x^b + M_y^b \delta K_y^b + M_{xy}^b \delta K_{xy}^b + M_x^s \delta K_x^s + M_y^s \delta K_y^s + M_{xy}^s \delta K_{xy}^s + Q_{yz}^s \delta\gamma_{yz}^s + Q_{xz}^s \delta\gamma_{xz}^s + N_x^0 \frac{\partial w}{\partial x}\frac{\partial \delta w}{\partial x} + N_y^0 \frac{\partial w}{\partial y}\frac{\partial \delta w}{\partial y} + 2N_{xy}^0 \frac{\partial w}{\partial x}\frac{\partial \delta w}{\partial y}] dA = 0 \quad (13)$$

where:

$$\begin{bmatrix} N_x, & N_y, & N_{xy} \\ M_x^b, & M_y^b, & M_{xy}^b \\ M_x^s, & M_y^s, & M_{xy}^s \end{bmatrix} = \int_{-\frac{h}{2}}^{\frac{h}{2}} (\sigma_x, \sigma_y, \tau_{xy}) \begin{bmatrix} 1 \\ z \\ f(z) \end{bmatrix} dz \quad (14)$$

$$(Q_{xz}^s, Q_{yz}^s) = \int_{-\frac{h}{2}}^{\frac{h}{2}} (\tau_{xy}, \tau_{yz}) g(z) dz$$

By integrating the displacement gradients by parts and setting the coefficients δu_o, δv_0, δw_b and δw_s to zero separately, the equilibrium equation associated with the present theory obtained is as follows.

$$\delta u : \frac{\partial N_x}{\partial x} + \frac{\partial N_{xy}}{\partial y} = 0 \quad (15)$$

$$\delta v : \frac{\partial N_{xy}}{\partial x} + \frac{\partial N_y}{\partial y} = 0$$

$$\delta w_b : \frac{\partial^2 M_x^b}{\partial x^2} + 2\frac{\partial^2 M_{xy}^b}{\partial x \partial y} + \frac{\partial^2 M_y^b}{\partial y^2} + N = 0$$

$$\delta w_s : \frac{\partial^2 M_x^s}{\partial x^2} + 2\frac{\partial^2 M_{xy}^s}{\partial x \partial y} + \frac{\partial^2 M_y^s}{\partial y^2} + \frac{\partial Q_{xz}^s}{\partial x} + \frac{\partial Q_{yz}^s}{\partial y} + N = 0$$

where:

$$N = N_x^0 \frac{\partial^2 (w_b + w_s)}{\partial x^2}$$

The stress resultants of a plate made up of three layers can be related to the total strains by substituting (10) in (14).

$$\begin{bmatrix} N \\ M^b \\ M^s \end{bmatrix} = \begin{bmatrix} A & B & B^s \\ B & D & D^s \\ B^s & D^S & H^s \end{bmatrix} \begin{bmatrix} \varepsilon \\ K^b \\ K^s \end{bmatrix}, Q = A^s \gamma \quad (16)$$

where:

$$N = \begin{bmatrix} N_x, & N_y, & N_{xy} & \end{bmatrix}^t, M^b = \begin{bmatrix} M_x^b, & M_y^b, & M_{xy}^b & \end{bmatrix}^t \quad (17)$$

$$M^s = \begin{bmatrix} M_x^s, & M_y^s, & M_{xy}^s & \end{bmatrix}^t$$

$$\varepsilon = \begin{bmatrix} \varepsilon_x^0, & \varepsilon_y^0, & \gamma_{xy}^0 & \end{bmatrix}^t, K^b = \begin{bmatrix} K_x^b, & K_y^b, & K_{xy}^b & \end{bmatrix}^t$$

$$K^s = \begin{bmatrix} K_x^s, & K_y^s, & K_{xy}^s & \end{bmatrix}^t$$

$$A = \begin{bmatrix} A_{11} & A_{12} & 0 \\ A_{12} & A_{22} & 0 \\ 0 & 0 & A_{66} \end{bmatrix}, B = \begin{bmatrix} B_{11} & B_{12} & 0 \\ B_{12} & B_{22} & 0 \\ 0 & 0 & B_{66} \end{bmatrix}$$

$$D = \begin{bmatrix} D_{11} & D_{12} & 0 \\ D_{12} & D_{22} & 0 \\ 0 & 0 & D_{66} \end{bmatrix}, B^s = \begin{bmatrix} B_{11}^s & B_{12}^s & 0 \\ B_{12}^s & B_{22}^s & 0 \\ 0 & 0 & B_{66}^s \end{bmatrix}$$

$$D^s = \begin{bmatrix} D_{11}^s & D_{12}^s & 0 \\ D_{12}^s & D_{22}^s & 0 \\ 0 & 0 & D_{66}^s \end{bmatrix}, H^s = \begin{bmatrix} H_{11}^s & H_{12}^s & 0 \\ H_{12}^s & H_{22}^s & 0 \\ 0 & 0 & H_{66}^s \end{bmatrix}$$

$$Q = \begin{bmatrix} Q_{xz}^s, & Q_{yz}^s \end{bmatrix}^t, \gamma = \begin{bmatrix} \gamma_{xz}, & \gamma_{yz} \end{bmatrix}^t$$

$$A^s = \begin{bmatrix} A_{44}^s & 0 \\ 0 & A_{55}^s \end{bmatrix}$$

where A_{ij}, B_{ij} etc are the plate stiffness defined by (18).

$$\begin{bmatrix} A_{11} & B_{11} & D_{11} & B_{11}^s & D_{11}^s & H_{11}^s \\ A_{12} & B_{12} & D_{12} & B_{12}^s & D_{12}^s & H_{12}^s \\ A_{66} & B_{66} & D_{66} & B_{66}^s & D_{66}^s & H_{66}^s \end{bmatrix} = \int_{-\frac{h}{2}}^{\frac{h}{2}} Q_{11}(1, z, z^2, f(z), zf(z), f^2(z)) \begin{bmatrix} 1 \\ \nu \\ \frac{1-\nu}{2} \end{bmatrix} dz \quad (18)$$

$$(A_{22}, B_{22}, D_{22}, B_{22}^s, D_{22}^s, H_{22}^s) = (A_{11}, B_{11}, D_{22}, B_{11}^s, D_{11}^s, H_{11}^s)$$

$$A_{44}^s = A_{55}^s = \int_{h_{n-1}}^{h_n} Q_{44}[g(z)]^2 dz$$

Substituting (16) in equilibrium equation (19) is obtained,

$$\begin{aligned} &A_{11}d_{11}u_0 + A_{66}d_{22}u_0 + (A_{12} + A_{66})d_{12}v_0 - B_{11}d_{111}w_b \\ &-(B_{12} + 2B_{66})d_{122}w_b - (B_{12}^s + 2B_{66}^s)d_{122}w_s \\ &-B_{11}^s d_{111}w_s = 0 \end{aligned}$$

$$\begin{aligned} &A_{22}d_{22}v_0 + A_{66}d_{11}v_0 + (A_{12} + A_{66})d_{12}u_0 - B_{22}d_{222}w_b \\ &-(B_{12} + 2B_{66})d_{112}w_b - (B_{12}^s + 2B_{66}^s)d_{112}w_s \\ &-B_{22}^s d_{222}w_s = 0 \end{aligned}$$

$$\begin{aligned} &B_{11}d_{111}u_0 + (B_{12} + 2B_{66})d_{122}u_0 + (B_{12} + 2B_{66})d_{112}v_0 \\ &+B_{22}d_{222}v_0 - D_{11}d_{1111}w_b - 2(D_{12} + 2D_{66})d_{1122}w_b \\ &-D_{22}d_{2222}w_b - D_{11}^s d_{1111}w_s - 2(D_{12}^s + 2D_{66}^s)d_{1122}w_s \\ &-D_{22}^s d_{2222}w_s + N_x^0 d_{11}w_b + N_x^0 d_{11}w_s = 0 \end{aligned}$$

$$\begin{aligned} &B_{11}^s d_{111}u_0 + (B_{12}^s + 2B_{66}^s)d_{122}u_0 + (B_{12}^s + 2B_{66}^s)d_{112}v_0 \\ &+B_{22}^s d_{222}v_0 - D_{11}^s d_{1111}w_b - 2(D_{12}^s + 2D_{66}^s)d_{1122}w_b \\ &-D_{22}^s d_{2222}w_b - H_{11}^s{}^s d_{1111}w_s - 2(H_{12}^s + 2H_{66}^s)d_{1122}w_s \\ &-H_{22}^s d_{2222}w_s + A_{55}^s d_{11}w_s + A_{44}^s d_{22}w_s \\ &+N_x^0 d_{11}w_b + N_x^0 d_{11}w_s = 0 \end{aligned} \quad (19)$$

where d_{ij}, d_{ijl} and d_{ijlm} are the following differential operators,

$$d_{ij} = \frac{\partial^2}{\partial_{xi}\partial_{xj}}, d_{ijl} = \frac{\partial^3}{\partial_{xi}\partial_{xj}\partial_{xl}}, d_{ijl} = \frac{\partial^4}{\partial_{xi}\partial_{xj}\partial_{xl}\partial_{xm}} \quad (20)$$

III. EXACT SOLUTION FOR A SIMPLY SUPPORTED FG PLATE

Rectangular plates are generally classified in accordance with the type of support used. For a simply supported FG plate, the following boundary conditions are imposed at the side edges:

$$\begin{aligned} v_0 = w_b = w_s = N_x = M_x^b = M_x^s = \frac{\partial w_s}{\partial y} = 0 \\ at, x = -a/2, a/2 \\ u_0 = w_b = w_s = N_y = M_y^b = M_y^s = \frac{\partial w_s}{\partial x} = 0 \\ at, y = -b/2, b/2 \end{aligned} \quad (21)$$

Following the Navier solution procedure, we assume the following solution form for u_0, v_0, w_b, and w_s, that satisfies the boundary conditions,

$$\begin{bmatrix} u_0 \\ v_0 \\ w_b \\ w_s \end{bmatrix} = \begin{bmatrix} U\cos(\lambda x)\sin(\mu y) \\ V\cos(\mu y)\sin(\lambda x) \\ W_b\sin(\lambda x)\sin(\mu y) \\ W_s\sin(\lambda x)\sin(\mu y) \end{bmatrix} \quad (22)$$

where $\lambda = \pi/a$, $\mu = \pi/b$ and U, V, W_b, W_s are arbitrary parameters to be determined subjected to the condition that the solution in (22) satisfies (19). Thus one obtains the operator equation (23),

$$[C]\{\Delta\} = 0 \quad (23)$$

where:

$$\Delta = \{U, V, W_b, W_s\}^t, [C] = \begin{bmatrix} a_{11} & a_{12} & a_{13} & a_{14} \\ a_{12} & a_{22} & a_{23} & a_{24} \\ a_{13} & a_{23} & a_{33} & a_{34} \\ a_{14} & a_{24} & a_{34} & a_{44} \end{bmatrix} \quad (24)$$

In which:

$$a_{11} = A_{11}\lambda^2 + A_{66}\mu^2$$

$$a_{12} = \mu\lambda(A_{12} + A_{66})$$

$$a_{13} = -\lambda[B_{11}\lambda^2 + (B_{12} + 2B_{66})\mu^2]$$

TABLE I FOR $\tilde{N}$ PFGM PLATE

b/h	CPT[2]	FSDT[2]	TSDT[2]	NHPSDT
10	17.6883	16.7678	16.7231	17.6457
20	17.6883	17.4489	17.3971	17.6441
40	17.6883	17.6279	17.5012	17.6448
50	17.6883	17.6496	17.5954	17.6457
100	17.6883	17.6786	17.6687	17.6457

TABLE II FOR $\tilde{N}$ SFGM PLATE

b/h	CPT[2]	FSDT[2]	TSDT[2]	NHPSDT
10	11.5459	10.9333	10.7421	11.4777
20	11.5459	11.3864	11.3124	11.5443
40	11.5459	11.5056	11.4786	11.5458
50	11.5459	11.5201	11.5174	11.5466
100	11.5459	11.5395	11.5352	11.5470

$$a_{14} = -\lambda[B^s_{11}\lambda^2 + (B^s_{12} + 2B^s_{66})\mu^2]$$

$$a_{22} = A_{66}\lambda^2 + A_{22}\mu^2$$

$$a_{23} = -\mu[B_{22}\mu^2 + (B_{12} + 2B_{66})\lambda^2]$$

$$a_{24} = -\mu[B^s_{22}\mu^2 + (B^s_{12} + 2B^s_{66})\lambda^2] \quad (25)$$

$$a_{33} = D_{11}\lambda^4 + 2(D_{12} + 2D_{66})\lambda^2\mu^2 + D_{22}\mu^4 + N^0_x\lambda^2$$

$$a_{34} = D^s_{11}\lambda^4 + 2(D^s_{12} + 2D^s_{66})\lambda^2\mu^2 + D^s_{22}\mu^4 + N^0_x\lambda^2$$

$$a_{44} = H^s_{11}\lambda^4 + 2(H^s_{11} + 2H^s_{66})\lambda^2\mu^2 + H^s_{22}\mu^4 + A^s_{44}\mu^2 + A^s_{44}\lambda^2 + N^0_x\lambda^2$$

For a non-trivial solution (i.e. to obtain the buckling load), the determinant formed by the coefficients of U, V, W_b,W_s is set to zero, this gives a characteristics equation the solution of which yields the critical buckling load N^0_x. The solution obtained can be used for all the three FGM plates PFGM, SFGM and EFGM.

IV. NUMERICAL RESULTS AND DISCUSSION

Buckling loads are calculated for a metallic ceramic FG plate comprising alumina and aluminium mixture for PFGM, SFGM and EFGM by substituting corresponding modulus of elasticity in the solution obtained. The material properties are shown below.

$$E_m = 70GPa, E_c = 380GPa, \nu = 0.3$$

First, results are compared with available ones for a square PFGM, SFGM and EFGM plate for material gradient index, n = 0.1 using CPT, FSDT and TSDT.

TABLE III FOR $\tilde{N}$ EFGM PLATE

b/h	CPT[2]	FSDT[2]	TSDT[2]	NHPSDT
10	8.2497	7.8631	7.3123	8.1861
20	8.2497	8.1495	8.0975	8.2326
40	8.2497	8.2244	8.2134	8.2453
50	8.2497	8.2335	8.2319	8.2468
100	8.2497	8.2456	8.2439	8.2490

A. Validation of Results

Non dimensionalized buckling load, $\tilde{N}$ when n = 0.1 for a square PFGM, SFGM and EFGM plate is as given in TABLE I,II,III respectively, where:

$$\tilde{N} = N^0_x b^2/E_m h^3 \quad (26)$$

The graphical representation for $\tilde{N}$ when n=10 in case of PFGM , SFGM and EFGM plate for different b/h values using different theories are as shown in Fig. 1, 2, 3 respectively. As the plate changes from a thin plate to medium thick plate the results obtained using NHPSDT is giving a good agreement with that obtained using other theories. Thus one of the assumptions of NHPSDT as it is for the medium thick plate is validated.

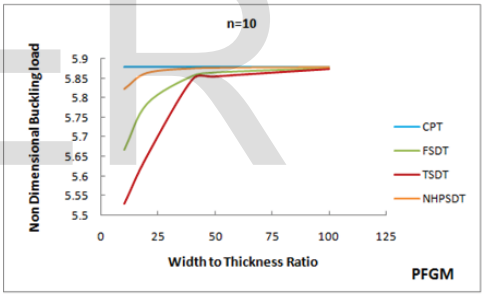

Fig. 1. Variation of $\tilde{N}$ with b/h for PFGM plate

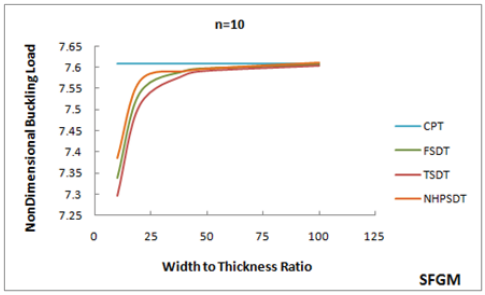

Fig. 2. Variation of $\tilde{N}$ with b/h for SFGM plate

B. Variation of $\tilde{N}$ with n value for different b/h ratio

The variation of $\tilde{N}$ with n value in case of SFGM plate for different b/h ratio are as shown in Fig. 4. As the value

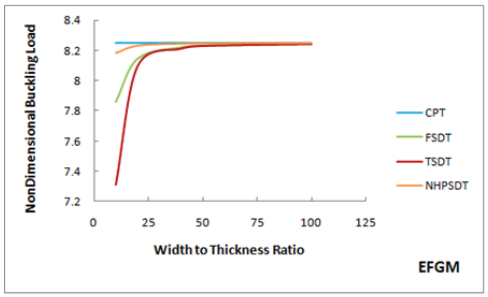

Fig. 3. Variation of Ñ with b/h for EFGM plate

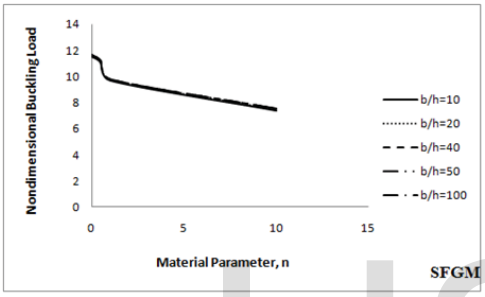

Fig. 4. Variation of Ñ with n value for different b/h ratio

of n increases there is decrease in Ñ value. This is due to the reason that at lower value of n the variation of material properties along the thickness of plate is gradual. As the value of n increases there is sudden change in the material properties along the thickness and so the Ñ value decreases. Also its clear that the effect of b/h on Ñ value is less when compared to the effect of n on Ñ.

C. Variation of Ñ with aspect ratio for different n values

Fig. 5 illustrate the variation of Ñ with aspect ratio 'a/b' for PFGM plates under uniaxial load. Results are based on NHPSDT only. The ratio of b/h of the plate is kept 20. The range of n is from 0.1 to 10. From Fig. 5 it can be inferred that

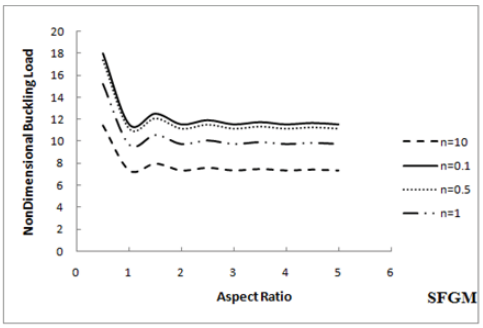

Fig. 5. Variation of Ñ with aspect ratio for SFGM plate

there is large difference in Ñ value when a/b less than one and beyond an a/b value of one, the Ñ value is almost constant. It is worthwhile to investigate whether the medium thick plate assumption will hold for FG plates with b/h ratio is 20 under

TABLE IV
VALUES OF a/h FOR DIFFERENT a/b WHEN $b/h = 20$

a/b	0.5	1	1.5	2	2.5	3	3.5	4	4.5	5
a/h	10	**20**	**30**	**40**	**50**	**60**	**70**	**80**	**90**	**100**

different a/b values. The length of plate 'a' is fixed and taken as 100cm. The width of plate 'b' is varying such that the aspect ratio a/b = 0.5, 1, 1.5 2. 2.5, 3, 3.5, 4, 4.5, 5. For each aspect ratio a/b, the thickness 'h' changes so that b/h value is 20. The b/h value corresponding to different a/b value when b/h = 20 are listed in TABLE IV in which bold entries indicate that the thickness satisfies the medium thick plate assumption ie; a/h = 20 - 100 approximately. For a/b greater than one when b/h = 20, the plate satisfies the assumption of medium thick plate and value of Ñ tends to a constant.

D. Effect of E1/E2 ratio on Ñ values for varying n

The effect of E1/E2 ratio on Ñ values for n varying from 0 to 10 when b/h =20 is as shown in Fig. 6. E2 is the modulus of elasticity of the material at the top of the plate and E1 is that at the bottom. As E1/E2 ratio increases the plate can deflect more due to the decrease in the stiffness of the plate. Thus it can take more load and Ñ value increases.

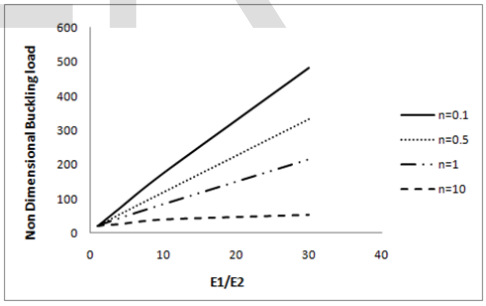

Fig. 6. Effect of E1/E2 ratio on Ñ values for varying n

V. COMPARISON OF THREE IDEALIZATION TECHNIQUES

A comparison of buckling loads obtained using three idealization techniques are as shown in Fig. 7. The length a of the plate is fixed as 1m and the thickness h is fixed as 0.1m. The width b changes with change in b/h ratio. The modulus of elasticity of the metallic phase adopted is 70 GPa (aluminium) and that of ceramic phase is 380 GPa (alumina). From Fig. 7 it is clear that the SFGM plate shows a greater nondimensional buckling load compared to the PFGM plate. In case of SFGM two power-law functions are used to describe the variation of Young's modulus across the thickness direction. Thus a smooth distribution of the material properties along the thickness was ensured. The largest value of the nondimensional buckling load obtained is by using exponential law due to the use of the exponential function to define the variation of Youngs modulus in the EFGM plates.

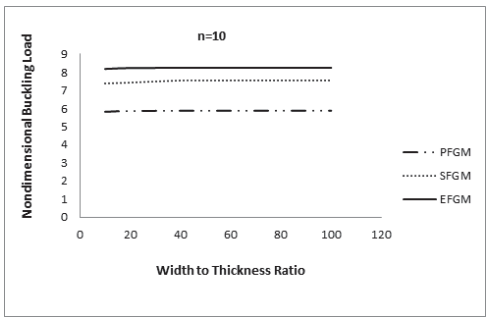

Fig. 7. Effect of b/h ratio on ˜N for P, S and EFGM plates

VI. COMPARISON OF SFGM PLATE WITH ISOTROPIC PLATE USING NHPSDT

A comparison study of the buckling behavior of SFGM plate with isotropic plate using NHPSDT is conducted. Here for the isotropic plate and for the SFGM plate the length a of the plate is fixed as 1m and the thickness h is fixed as 0.1m. The width b changes with change in b/h ratio. For the isotropic plate with

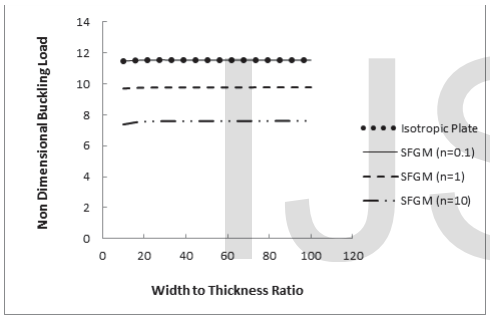

Fig. 8. Comparison of ˜N for SFGM plate with isotropic plate using NHPSDT

E1/E2 ratio equal to one has higher value of nondimensional buckling load when compared to that of other FGM plates. The nondimensional buckling load obtained by an SFGM plate for a material parameter less than one (n=0.1) coincides with that obtained for an isotropic plate. Thus the buckling load of an isotropic plate is same as that of an SFGM plate for the material parameter less than one due to the sudden change in the material properties of SFGM towards the top portion of the plate. For a material parameter greater than one (n=10) nondimensional buckling load obtained by an SFGM plate shows a lesser value compared to an isotropic plate.

VII. CONCLUSION

1) The closed form solution obtained using the New Hyperbolic Shear Deformation Theory can be effectively used for the buckling analysis of medium thick FGM plate with simply supported end conditions under uniaxial inplane compressive force.
2) For a/b / 1, the PFGM, SFGM and EFGM plates show a rapid increase in the nondimensional buckling load whereas for a/b V 1, nondimensional buckling load approaches to a constant value validating the medium thick plate assumption for New Hyperbolic Shear Deformation Theory.
3) As E1/ E2 ratio increases the critical buckling load increases. This is because of the decrease in stiffness of the FGM plate with increase in E1/ E2 ratio leading to an increase in the buckling load of FGM plates.
4) As the value of the material parameter 'n' increases the nondimensional buckling load decreases. This is due to the reason that at lower value of n, (n/1) the variation of material properties will be rapid towards the top portion of plate whereas the material properties changes rapidly towards the bottom portion of the plate for n V 1.
5) The EFGM plate shows a larger value of non dimensional buckling load compared to PFGM and SFGM plate. This is due to the use of the exponential function to define the variation of Youngs modulus in the EFGM plates.
6) The material parameter n has no effect on the buckling of EFGM plates.
7) The SFGM plate shows a greater non dimensional buckling load compared to the PFGM plate. This is due to the usage of two power-law functions to define the variation of Youngs modulus, ensuring a smooth variation of the material properties throughout the thickness direction
8) The non dimensional buckling load obtained by an SFGM plate for material parameter 'n' less than one coincides with that obtained for an isotropic plate, due to the sudden change in the material properties towards the top portion of the SFGM plate.
9) For a material parameter 'n' greater than one the nondimensional buckling load obtained by an SFGM plate shows a large variation with that of the isotropic plate.
10) The New Hyperbolic Shear Deformation Theory can be used for the buckling analysis of a medium thick FG plate with an advantage of having only four unknowns against five as in case of other shear deformation theo-ries.

Acknowledgement

The authors would like to thank all faculties of the department of civil engineering, Mar Basaelios college of Engineering and Technology, Trivandrum. They are also grateful to all who have helped them in the course of the study.

References

[1] Tahar Hassaine Daouadji, Abdelouahed Tounsi and E.I Abbes Adda Bedia, "Analytical solution for Bending analysis of Functionally Graded Plates", Scientia Iranica, Vol. 20, pp. 516-523, February 2013.
[2] Rohit Saha and P. R. Maiti, "Buckling of simply supported FGM plates under uniaxial load", International journal of civil and structural engineering, Vol. 2, pp. 1035-1049, 2012.
[3] Shyang Ho Chi and Yen Ling Chung, "Mechanical behavior of Functionally Graded material plates under Transverse load - Part I: Analysis", International journal of solids and structures, Vol. 43, pp. 3657-3674, June 2005.
[4] Shyang Ho Chi and Yen Ling Chung, "Mechanical behavior of Function-ally Graded material plates under Transverse load - Part II: Numerical results", Applied Mathematical Modelling, Vol. 37, pp. 3269-3281, 2013. thic

[5] Huu-Tai Thai and Thuc P. Vo, "A New Sinusoidal Shear Deformation Theory for Bending, Buckling and Vibration of Functionally Graded plates", International journal of solids and structures, Vol. 43, pp. 3675-3691, June 2005.

[6] D.K. Jha, Tarun Kant and R.K. Singh, "A Critical Review of recent research on Functionally Graded plates", Composite structures, Vol. 96, pp. 833-849, 2013.

[7] S. Brischetto and E. Carrera, "Advanced Mixed Theories for Bending analysis of Functionally Graded plates", Computers and structures, Vol. 88, pp. 1474-1483, 2010.

Strength and Durability of OPC-Fly Ash-Sugarcane Bagasse Ash Blended Concrete

Vishnumaya L, Rekha Ambi
Dept. of Civil Engineering
TKM College of Engineering
Kollam – 691005, India.
e-mail: vishnumaya.rit@gmail.com ,
rekha_ambi@hotmail.com

Abstract— **Concrete is an important and commonly used man made construction material, which can be considered to have better strength and durability characteristics. Nowadays, ternary blended concrete is achieving popularity by overcoming the disadvantages of binary blended concrete. The present work deals with study of fresh properties, strength, and durability of ternary blended concrete with Fly Ash and Sugarcane Bagasse Ash (SCBA). Concrete mix is designed for strength of 30MPa. The study is limited to ternary blended concrete with 30% replacement of cement with Fly Ash and remaining cement is replaced with 5%, 10%, 15%, 20%, 25 %and 30% of SCBA in different mixes. The tests on hardened concrete were destructive in nature which includes compressive test, flexural strength, modulus of elasticity, split tensile strength and impact resistance test. Durability tests are carried for which the specimens were exposed to the respective chemical condition for a time period of 56 and 90 days. Durability study includes sulphate resistance, and bulk diffusion. From the above tests conducted, the cement replaced by 30% fly ash and 10% SCBA showed better results. From the results, it can be concluded that the SCBA is a valuable pozzolanic material and it can be potentially be used as a partial replacement for cement. Up to 10% SCBA in concrete can be considered as the optimum replacement level with the addition of 30% fly ash by weight of cement.**

Keywords— Sugarcane Bagasse Ash;FlyAsh;strength;durability

I. INTRODUCTION

The infrastructure need of our country is increasing day by day and with concrete as a main constituent of construction material and the safety of systems is to be ensured. Cement is a prime ingredient for concrete based construction but its over usage leads to environmental pollution. Therefore, the cement demand needs to be reduced to decrease environmental pollution from cement industry. Moreover the unit cost of concrete can also be reduced by partial replacement of cement with some industrial by product. In the past, many researchers used different popular industrial by-products such as fly ash, ground granulated blast-furnace slag, silica fume, and natural pozzolans, such as calcined shale, calcined clay or metakaolin in conjunction with portland or blended cement to improve the properties of ordinary concrete. With the ever increasing demand and consumption of cement and in the backdrop of waste management, scientists and researchers all over the world are always in quest for developing alternate binders that are environment friendly and contribute towards sustainable management. Today researches all over the world are focusing on ways of utilizing agricultural wastes as a source of raw materials for the construction industry. Sugar-cane bagasse is one such fibrous waste-product of the sugar refining industry, along with ethanol vapor. Bagasse ash mainly contains aluminium ion and silica. Nowadays, ternary blended concrete is achieving popularity by overcoming the disadvantages of binary blended concrete. The present work deals with study of fresh properties, strength, and durability of ternary blended concrete with Fly Ash and Sugarcane Bagasse Ash (SCBA). The objective of the present study is to design a control mix blended with 30% fly ash as cement replacement and also to arrive at an optimum dosage of SCBA in fly ash blended concrete by studying the fresh properties, hardened properties and durability properties for different percentage of SCBA 5, 10, 15,20,25 and 30% by weight of cement.

II. EXPERIMENTAL PROGRAMME

A. Materials

Detailed tests were conducted in the laboratory to evaluate the required properties of the individual materials. Properties of the constituent materials were tested as per the methods prescribed by the relevant IS codes.

***Cement*:** Ordinary Portland cement (OPC) confirming to IS 12269 (53 Grade) was used for the experimental work. Laboratory tests were conducted on cement to determine specific gravity, fineness, standard consistency, initial setting time, final setting time and compressive strength. The results are presented in Table 1.

TABLE I PROPERTIES OF CEMENT

Sl No.	Particulars	Values
1	Grade	OPC 53 grade
2	Specific Gravity	3.13
3	Fineness	4%
4	Standard Consistency	30.5%
5	Initial Setting Time	90 mins
6	Final Setting Time	270 mins

Fly Ash: Low-calcium, Class F, dry fly ash with specific gravity 2.08, obtained from the silos of Tuticorin Thermal Power Plant in Tamil Nadu is to be used as binder. 70% of flyash was passing through the 45μm sieve. Wet sieve analysis was conducted as per IS 3812(part1):2003[11].

***Sugarcane Bagasse Ash*:** SCBA was collected during the cleaning operation of a boiler operating in the Sakthi Sugar Factory, located in the city of Sathyamangalam, Tamilnadu. Specific gravity of SCBA was determined as 2.16.The fineness was determined as 18%.

***Fine aggregate*:** Manufactured sand having fineness modulus 3.06 and specific gravity 2.50 was used as fine aggregate. Tests are conformed to IS: 383-1970[12].

***Coarse aggregate*:** Crushed stone aggregate of size between 20mm and 4.75mm and specific gravity 2.80 and fineness modulus 7.09 was used as coarse aggregate. Tests are conformed to IS: 383-1970[12].

***Water*:** Clean drinking water available in the college water supply system was used for mixing and preparing alkaline liquid.

Superplasticizer: The superplasticizer used was Ceraplast-300.

MIX PROPORTION

Mix proportion was arrived through various trial mixes. The grade of concrete prepared for the experimental study was M30. The proportion used in the investigation, after necessary adjustments made on the trial mixes, is shown in Table 2.The mix designation is shown in Table 3.

TABLE 2. MIX PROPORTION

Grade of concrete	Mix Proportion			
M30	C	FA	CA	w/c
	1	1.786	3.21	0.43

TABLE 3. MIX DESIGNATION

Mix Designation	Cement(%)	Fly Ash (%)	SCBA (%)
C	100	0	0
FB0	70	30	0
FB5	65	30	5
FB10	60	30	10
FB15	55	30	15
FB20	50	30	20
FB25	45	30	25
FB30	40	30	30

C. Methods

Workability: The workability was assessed by determining the compacting factor as per the **IS 1199:1959** [13] specification.

***Compressive strength*:** In the present study, compression tests were carried out on 100mm cube specimens at ages of 3, 7, 28, 56 and 90 day as per **IS:516-1959** [14]**.** The reported strength values are average of three test results.

***Flexural Strength Test*:** Flexural strength test was conducted as per **IS: 516-1959**.The standard beam specimens of size 500 x 100 x 100 mm were used for this investigation. Two-point loading was applied and breaking load was noted at 28th day.

Split Tensile Strength Test: The split tensile test is a well known indirect test used for determining the tensile strength of concrete. Test was carried out on concrete cylinder of size 150mm×300mm as per IS 5816:1999 specification.

Modulus of Elasticity: The modulus of elasticity was determined by subjecting cylinder specimen having 150 mm diameter and 300 mm height to uniaxial compression as per IS 516:1959 specification.

Impact Resistance:Impact resistance is one of the important attributes of concrete. According to this test, impact resistance is characterized by a measure of the number of blows in a repeated impact test to achieve a prescribed level of distress.

***Sulphate Resistance Test*:** The test was conducted based on ASTM C 452-02[15] test method. After 56 days and 90 days of 20000ppm magnesium sulphate exposure, 100mm cube specimens were tested for compressive strength.

Bulk diffusion test: The test proposes to assess the chloride attack on concrete specimen by measuring the depth of chloride penetration into the concrete specimen. In this test, cylinder of 100 mm diameter and 200mm length was used as test specimen. After 7 days of water curing, the concrete specimens were exposed to 1.8 Molar NaCl solution for 56 days and 90 days. After 56 days and 90 days of exposure the specimens were split by applying splitting tensile force. To the split face, 0.1 Molar Silver Nitrate ($AgNO_3$) solution was sprayed to observe the colour changes ie, up to the penetrated depth of chloride ion, a white precipitation will form and thus the depth of chloride ions can be found out.

II. RESULTS AND DISCUSSIONS

This session provides a summary of the experimental results and endeavours to draw some conclusions. The test result covers the workability, mechanical properties and durability properties geopolymer concrete with and without steel fibres.

Workability: The results showed that the workability was decreasing wiyh increasing percentage of SCBA. Inorder to get workability concrete with SCBA needs higher water content than a concrete without SCBA.The probable reason may be higher specific surface area of SCBA and its lower density resulting in a higher porosity which requires higher water demand.

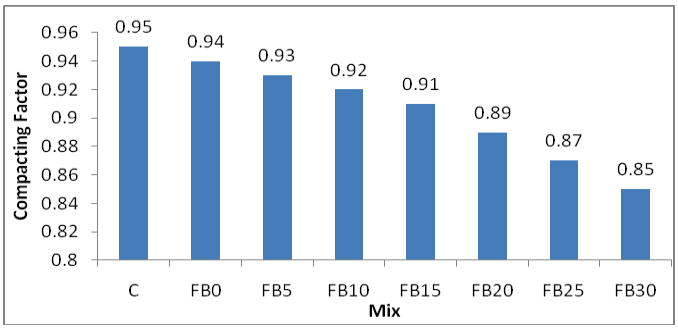

Fig. 1 Compacting factor variation

Compressive Strength test: For each mix, three cube specimens of size 150mm×150mm×150mm were tested for compressive strength. Cubes were tested after 3, 7, 28, 56 and 90 days of water curing. The control mix showed greater early age strength (3 days and 7 days) compared to the mix with 30% replacement of fly ash only, but its long term strength was higher than the control mix. When fly ash is added to concrete, fly ash plays the dual role of fine aggregate and cementitious component. In the earliest stages of curing, it acts as an inert fine aggregate, but in the presence of moisture, the silica and alumina of the fly ash gradually react with the calcium hydroxide released in the hydration of Portland cement. As the fly ash combines with the calcium hydroxide, it slowly converts it to calcium silicate and calcium aluminate binders. This chemical reaction occurs much more slowly than the hydration of Portland cement. Because the reaction proceeds slowly, the full potential strength of fly ash concrete may not be attained at early ages. The ternary mixes up to 15% replacement level showed strength comparable to the control mix at early ages. The mixes up to 20% replacement level showed higher early age strength compared to FB0.Among the ternary mixes FB10 showed better strength compared to control mix and FB0 at all ages. The higher replacement of cement by SCBA reduces cement content of mixture which in turn results in reduction of hydration reaction. Also the higher content of SCBA resulted in a higher water requirement, making water unavailable for hydration of cement and reducing hydration and compressive strength development. The increase in compressive strength of FB10 is 13.46% than the control mix and 9.89% than FB0 after 28 days. The increase in compressive strength in the presence of 10% SCBA may be both due to physical and chemical processes. It may lead to the segmentation of large capillary pores. It may introduce a large number of nucleation sites in the system for rapid precipitation of hydration products.

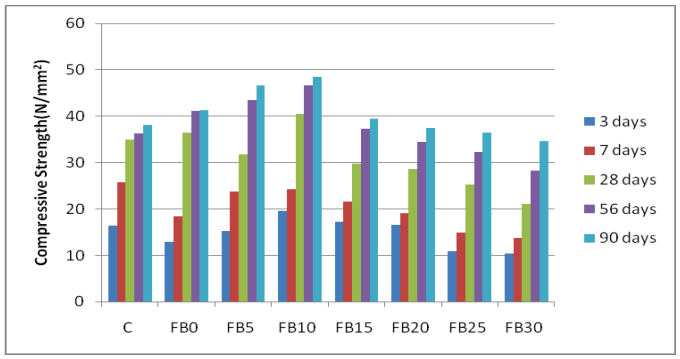

Fig. 2 Compressive strength variation for different mixes

Flexural strength Test: The maximum flexural strength is obtained for ternary mix with 10% SCBA replacement. The mixes up to 25% replacement level showed a greater flexural strength than the control mix. It may due to large pozzolanic reaction and improved interfacial bond between paste and aggregates.Fig 3 shows the variation of flexural strength for different mixes.

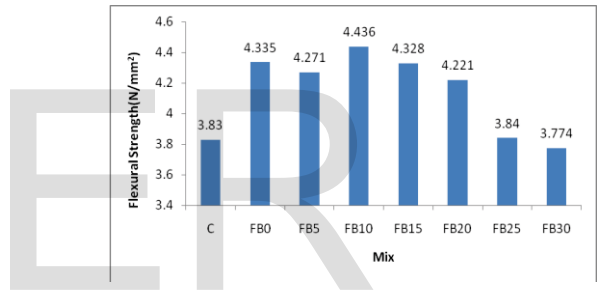

Fig.3 Variation of flexural strength for different mixes

Split Tensile Strength Test:Fig. 4shows the result of split tensile strength of all mixes after 28 days of water curing. The maximum tensile strength is obtained for FB10 mix with 10% replacement of SCBA and the result is comparable to FB0 mix. The mixes up to 25% replacement level showed greater strength than the control mix. The greater strength may due to grain and pore refinement of concrete resulted from very high fineness of particles and pozzolanic reaction of ashes

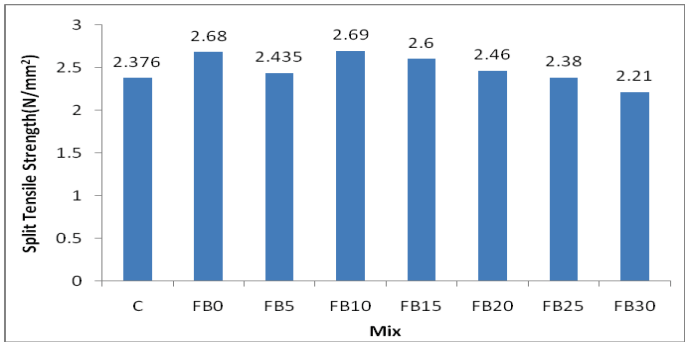

Fig.4 Variation of Split tensile strength for different mixes

Modulus of elasticityThe Young's modulus values are obtained from stress-strain diagram obtained by carrying out the test on 150mm × 300mm cylinders. Fig 5 shows the